CyclObs Database

Validation report - Part 1: Main report

Alexis Mouche (IFREMER)
Théo Cévaer (OceanScope)
Olivier Archer (IFREMER)

Ifremer

CyclObs Database
Validation report - Part 1: Main report

by

Alexis Mouche (IFREMER)
Théo Cévaer (OceanScope)
Olivier Archer (IFREMER)

Document version   1.0
Institution: Institut Français de Recherche
                    pour l'Exploitation de la MER
Document Date: Monday 21st March, 2022

Contents

1

CYMS and reference products

This section is a brief overview of the CYMS products to monitor tropical cyclones with SAR and data used for comparison.

1.1. CYMS products

This section presents CYMS products and associated key variables that are validated in this document. In particular we focus on

- Level-2 ocean surface wind product from CyclObs archive
- Tropical Cyclone Vortex Analysis product (TCVA products)

1.1.1. Level-2 CyclObs ocean surface wind product

Level-2 CyclObs wind product main variable is the wind speed. A Level-2 CyclObs wind product can be composed of several successive Level-1 SAR acquisitions. Each Level-1 acquisitions is processed into a Level-2 wind products. An example of two simultaneous of Sentinel-1B SAR acquisitions with VV and VH polarizations over Veronica tropical cyclone (south-indian ocean in 2019) on 2019-03-23 between 21:38:33 and 21:39:52 UTC is presented on figure 1.1.
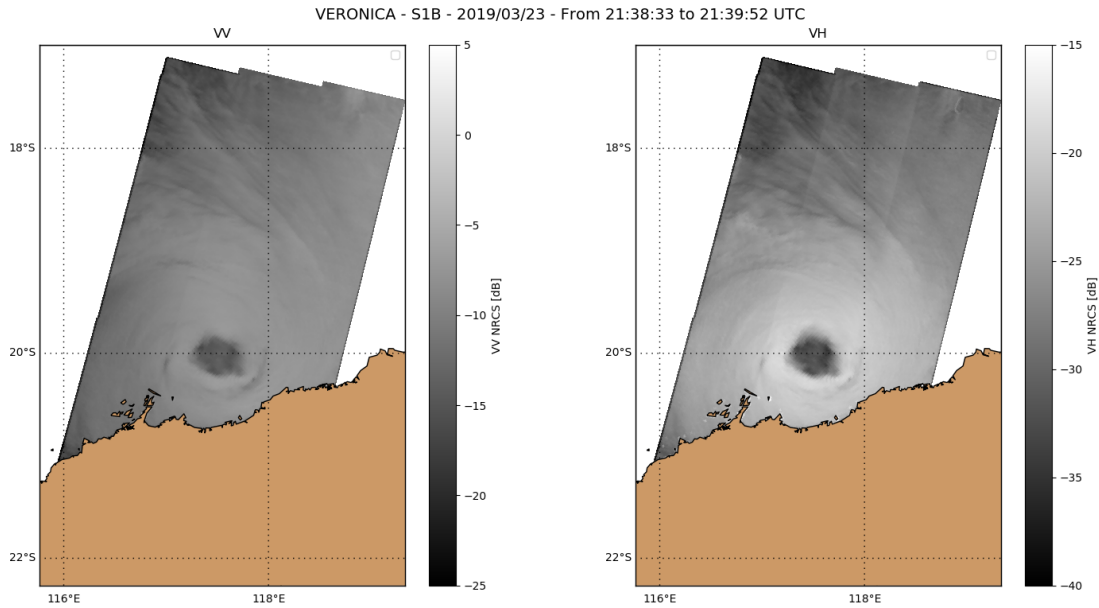
Figure 1.1: Example of Sentinel-1B SAR acquisitions over Veronica tropical cyclone on 2019-03-23 between 21:38:33 and 21:39:52 UTC. Left: Radar cross-section map in co-polarization (VV). Right: Radar cross-section map in cross-polarization (VH).

These products are then concatenated into a single Level-2 product. The wind can be processed at different resolutions from 1 to 50 km with a 1 km pixel spacing.

There are two versions of the product

- SAR Ocean Surface Wind along track (or swath) Level-2 product based on Radarsat-2, Sentinel-1A and Sentinel-1B measurements.
- SAR Ocean Surface Wind gridded Level-2 product based on Radarsat-2, Sentinel-1A and Sentinel-1B measurements

The wind estimate relies on the use of both VV and VH channels. VV-NRCS is known to be very robust for wind vector estimates from low to high wind regimes, with low signal-to-noise ratio and sensitivity to ocean wind direction. Whereas VV-NRCS sensitivity is decreasing under more extreme conditions, VH-NRCS still exhibits significant sensitivity(Zhang and Perrie, 2012). Algorithm for Level-2 CyclObs wind product combines SAR information with a priori information. VV-NRCS and VH-NRCS measurements are combined with ocean wind vector from ECWMF (spatial resolution is 0.125° with a time step of 3 h) to provide a wind speed estimate. Gaussian errors are considered for observations, geophysical model function (GMF) used to relate NRCS to wind speed and direction as a function of radar parameters, and the model information. This leads to a minimization problem for the determination of the maximum probability to get a wind vector (speed and direction). For each NRCS measurements couple (VH and VV), the cost function to minimize writes:

$$
J(u_{10}, v_{10}) = \left[\frac{u_{10}^{a\,priori} - u_{10}}{\Delta u_{10}} \right]^2 + \left[\frac{v_{10}^{a\,priori} - v_{10}}{\Delta v_{10}} \right]^2 + \sum_{\mathrm{pp} \in [\mathrm{VV,VH}]} \left[\frac{\sigma_0^{\mathrm{pp}} - \mathrm{GMF}^{\mathrm{pp}}(\theta, \phi, U_{10})}{\Delta \sigma_0^{\mathrm{pp}}} \right]^2, \quad (1.1)
$$

where $\{u_{10}, v_{10}\}$ defines the space of solution in the geographical referential from -80 to 80 m/s and $\{\Delta u_{10}, \Delta v_{10}\}$, the associated errors. $u_{10}^{a\,priori}$ and $v_{10}^{a\,priori}$ are the *a priori* solution given by ECMWF model. σ_0^{pp} and $\Delta \sigma_0^{\mathrm{pp}}$ are respectively the NRCS measurements in co- (pp = VV) and cross- (pp = VH) polarization and the associated errors. $\mathrm{GMF}^{\mathrm{pp}}(\theta, \phi, U_{10})$ stands for the GMF defined for each polarization with respect to incidence angle θ, wind direction relative the antenna look direction ϕ and wind speed U_{10}. Figure 1.2 provides an example of CyclObs Level-2 SAR ocean surface wind speed map for Veronica TC obtained from Level-1 observations presented on Figure 1.1.

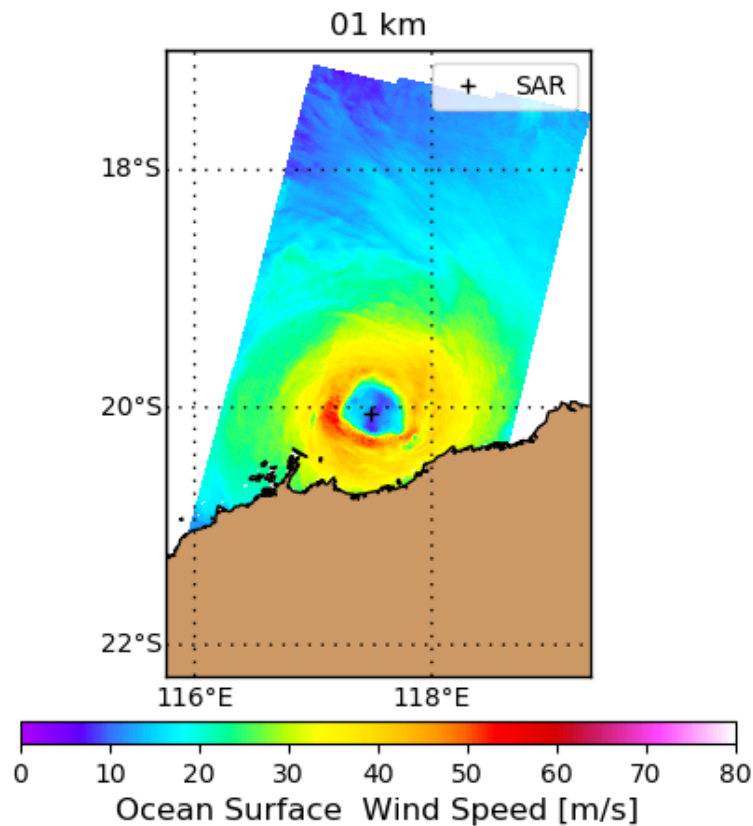VERONICA - S1B - 2019/03/23 - From 21:38:33 to 21:39:52 UTC

Figure 1.2: Example of CyclObs Level-2 ocean surface wind speed obtained from Sentinel-1B SAR acquisitions in dual polarization over Veronica tropical cyclone on 2019-03-23 as presented on Figure 1.1

1.1.2. Tropical Cyclone Vortex Analysis product
TO BE DONE.

1.2. Reference Product

1.2.1. SFMR
Rain rates and ocean surface wind speeds from the SFMR are used as independent measurements. Since its first experimental flight in 1980 through Hurricane Allen, SFMR is now installed on all U.S. hurricane reconnaissance aircraft to routinely and operationally provide wind and rain estimates during TC events. Airplanes fly directly into the eye of the hurricane, usually adopting an "alpha" or "multi-alpha" pattern, to best sample the four geographical quadrants. An example of such pattern is shown on Fig. 1.3 when the airplane was flying into Irma TC on September 7 2017. The background are maps of SAR acquisitions occurred during this flight for the two polarization channels (see VV on Fig. 1.3 (a) and VH on Fig. 1.3 (b)). The SFRM concept relies on the use of a C-band radiometer operating at six different frequencies ranging from 4.5 to 7.2 GHz with different sensitivities to foam coverage at the sea surface (related to ocean surface wind speed) and to rain (Uhlhorn and Black, 2003).

Over the course of time, retrieval algorithms have been further improved, as the possibilities to refine the filtering of the data and better describe the brightness temperature dependency to wind and rain increase with the number of available flights (Uhlhorn et al., 2007; Klotz and Uhlhorn, 2014). Recently, Sapp et al. (2019) proposed new improvements including a bias correction to calibrate the whole dataset, a new model for flat surface emissivity (Meissner and Wentz, 2012), a new frequency dependence for the atmospheric transmissivities, leading to a new method and formulation to derive the relationship between the wind excess emissivity and the ocean surface wind speed (so called wind GMF, for Geophysical Model Function). In particular, arguing on possible non-geophysical contamination of the lower-frequency channel, the highest frequency channel has been considered to derive a new wind
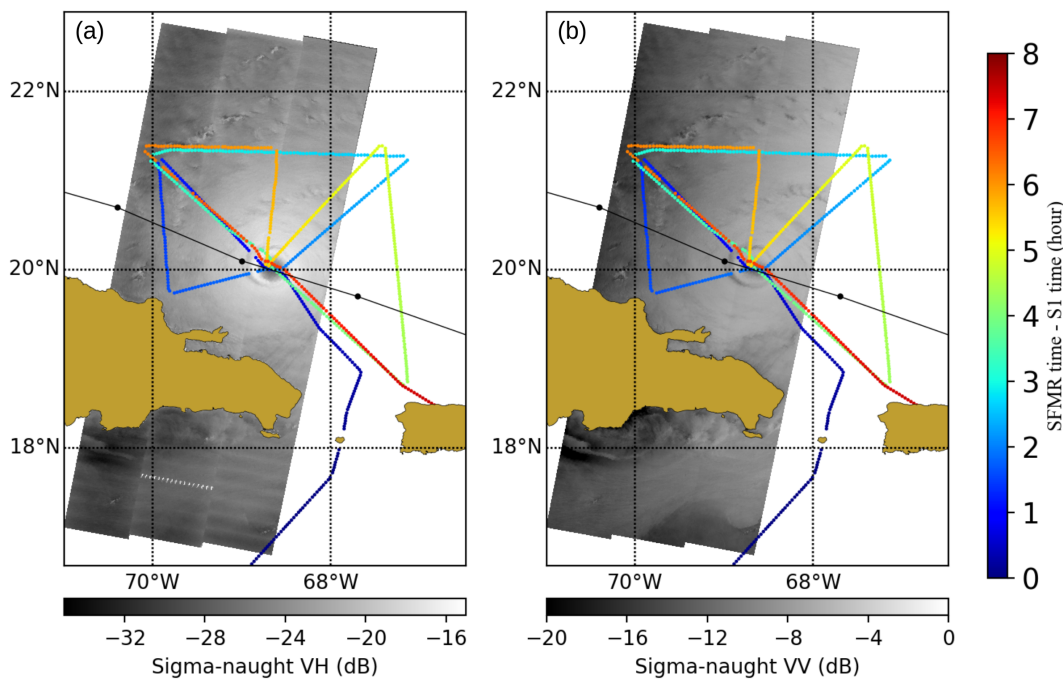
Figure 1.3: Maps of Normalized Radar Cross Section (NRCS) as measured by Sentinel-1 A over Irma category 5 hurricane on September 7, 2017. (a) NRCS in VV polarization. (b) NRCS in VH polarization. The locations of SFMR measurements after collocation are overlaid with color code indicating SFMR-derived ocean surface wind speed.

GMF (and its frequency dependency). This also imposed modification of the rain absorption model coefficient to maintain the initial rain rates performances (Klotz and Uhlhorn, 2014). Overall, SFMR wind speeds are expected to be higher than operational products for wind speeds larger than 15 m/s and are judged as non reliable for rain rates measurements larger than 45 mm h^{-1} (Sapp et al., 2019). This study does not aim to discuss the two existing SFMR products, and mainly relies on products processed and provided by NOAA/NESDIS (Sapp et al., 2019). For sake of completeness, results obtained with AOML/HRD products are also considered.

Because the SFMR design involves a single nadir-viewing antenna, only transects are available. Despite these limitations, the combined estimates of rain rate and ocean surface wind speed at very high resolution (temporal resolution is 1 second) makes this instrument unique for validating SAR-derived wind speeds and to discuss the possible rain impacts, especially in the TC inner core.

1.2.2. Tropical Cyclone Best-Track

SAR versus SFMR : Overview

2.1. Collocation

This section presents the collocation method and collocated data set available for comparisons.

2.1.1. Method

The two main differences between SAR and SFMR observations are (i) the duration required to sample a given TC and (ii) the coverage of the TC structure. For the Irma TC case presented in Figure 1.3, SAR data is acquired in less than three minutes, while the SFMR data collection lasts more than 9 hours. While the "multi-alpha" reconnaissance pattern (the solid purple line) is designed to sample the 2-D aspects of the TC, it can only do so in a low spatial resolution and temporally averaged manner. Thus a specific method has been developed.
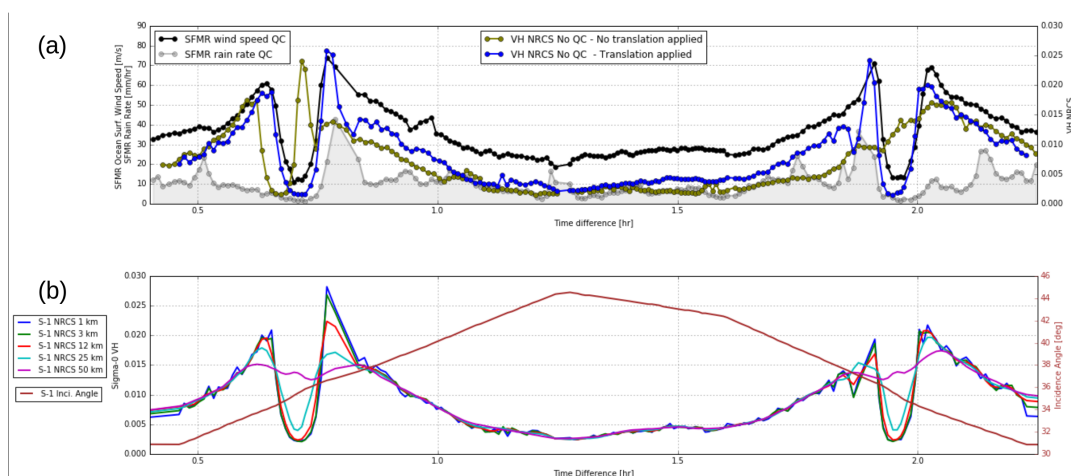

Figure 2.1: Transect of collocated SFMR and SAR measurements at 3 km resolution for Irma case presented on Fig 1.3. (a) Quality-controlled SFMR ocean surface wind speed (black) and rain rate (grey). NRCS in VH polarization with (blue) and without (olive) taking into account for Irma translation speed during the collocation (b). Same Sentinel-1 A NRCS transect than in (a) but for different resolutions (1, 3, 12.5, 25 and 50 km). Variation of SAR incidence angle along the transect is indicated in brown (right y-axis).

The collocation of rain and ocean surface wind speed measurements involves several steps (Mouche et al., 2019). First, SFMR measurements are smoothed using an averaging moving window of 10 seconds and a spatial re-sampling at 3 km. During this pre-processing step, the quality flag included in SFMR data can be used to possibly filter out low-quality data. Second, the hurricane translation speed is computed from the hurricane track. The location of SFMR measurements are then shifted with respect to the time difference between each SFMR measurements and the SAR acquisition time using the TC motion vector. The duration of a SAR acquisition is typically few seconds whereas a flight with

SFMR can last up to 6 hours and more. SAR time is thus considered constant with respect to SFMR times. Starting acquisition time is used for SAR acquisition time. If several acquisitions performed in a row are necessary to describe the whole hurricane, the duration of SAR acquisitions increases. For instance, in the case of Irma presented on Figure 1.3, a total of 4 successive acquisitions are concatenated to produce the image, leading to an acquisition duration of 1 minutes and 29 seconds. Finally, for each SFMR storm-motion-relative location, oceanic SAR measurements are averaged within a radius R. Note that this step results in a collocated SAR dataset with a pixel-spacing of 3 km but a spatial resolution depending on R. In this study we used $R = $ 1.5, 2.5, 6, 12.5 and 25 km to mimic different spatial resolutions.

An example of collocation obtained for Irma between Sentinel-1 A and SFMR is given Figure 2.1. Fig. 2.1 (a), shows the SFMR ocean surface wind speed and rain rate estimates as a function of time. Here the quality flag included in the SFMR data has been taken into account. X-axis indicates the time difference with respect to SAR acquisition time. In the present study, we only focused on collocations with an absolute time differences less than 2.5 hours. In this case, measurements up to 75 m/s have been measured by SFMR. These large values of wind speed strongly correlated with the highest values of rain rate, corresponding the western part of the TC eye, very close to RMW. The non-flagged observations appear to contain wind estimates where rain rates, which are discussed later, are up to 40mm/hr. To note, flagged measurements reach rain rates up to 80 mm/hr. This suggests that the quality procedure removes measurements for the most intense rain rates. Figure 2.1 (a) also presents the collocated cross-polarized NRCS (blue) with respect to time corresponding to the same SFMR measurements. As observed and already reported with SAR data from Radarsat-2 mission, there is a very strong correlation between SFMR ocean surface wind speeds and cross-polarized NRCS at C-Band (Zhang and Perrie, 2012). Figure 2.1 (a) also shows the match-ups that result if the collocation procedure is not performed. The olive line shows NRCS that has not been aligned with TC motion. In this case the strong correlation between SAR and SFMR measurements is completely lost.

The impact of the different spatial resolutions is presented on Figure 2.1 (b). This comparison shows the benefit of high resolution compared to medium resolution missions such as L-band radiometers (about 40 km for SMAP (Meissner et al., 2017; Yueh et al., 2016) or SMOS (Reul et al., 2016, 2017)) or scatterometers (about 25 km for nominal resolution with the next European SCA on MeTop SG (Stoffelen et al., 2017)). In this case, larger averaging areas blur the interpretation of the data; clearly showing that both the central wind minimum and peakedness of the wind maxima are severely impacted at spatial resolutions exceeding 12 km. In fact, at the time of acquisition, Irma eye diameter was about 30 km (about 16 nautical miles) as given by the Best-Track analysis, corresponding to less than 3 measurements at 25 km resolution. When the pixel sampling decreases, results are even worse (not shown). More generally, the use of SAR acquisitions with NRCS computed at different resolutions to systematically mimic lower resolution sensors can certainly help to characterize the resolution impact on the measurements depending on TC characteristics, particularly in the high wind-speed gradient areas near the RMW.

2.1.2. Dataset

When considering all SFMR wind and rain products available from NOAA/NESDIS and NOOA/HRD, we obtain 89 and YY collocations with SAR data. As observed on the map of Figure 2.2, available collocations are in the gulf of Mexico (27%), north Atlantic (east coast of the United States of America) (26%), Caribbean sea (25%) and north east Pacific (around Hawaii) (19%). The color code denotes the SAR sensor. Overall, SFMR provides

- 38 collocations with Radarsat-2.
- 32 with Sentinel-1A
- 19 with Sentinel-1B

. All TC categories are sampled

- cat-1: 19, i.e 21%;
- cat-2: 9, i.e. 10%;
- cat-3: 20, i.e. 22%;
- cat-4: 22, i.e. 24%;

- cat-5: 5, i.e. 5%

Figure 2.2 illustrates that the first significant collocations with SFMR obtained with Sentinel-1 missions have been obtained in 2016 and years after, 2016 being the starting date of the SHOC campaign. This clearly proves the benefit of this strategy. To note while 2018 and 2019 are the two years with the maximum numbers of SAR acquisitions over TC (about 150 and 120, respectively), 2020 is the year for which we have the maximum of SFMR/SAR collocations whereas less than 100 SAR acquisitions over TC were performed. In addition, although 2021 had the same number of SAR acquisitions over TC, the number of collocations is significantly smaller. This can be explained by the fact that airplanes flights are not worldwide in the contrary of SAR and that there is no phasing between the 3 SAR missions and airplanes flights.
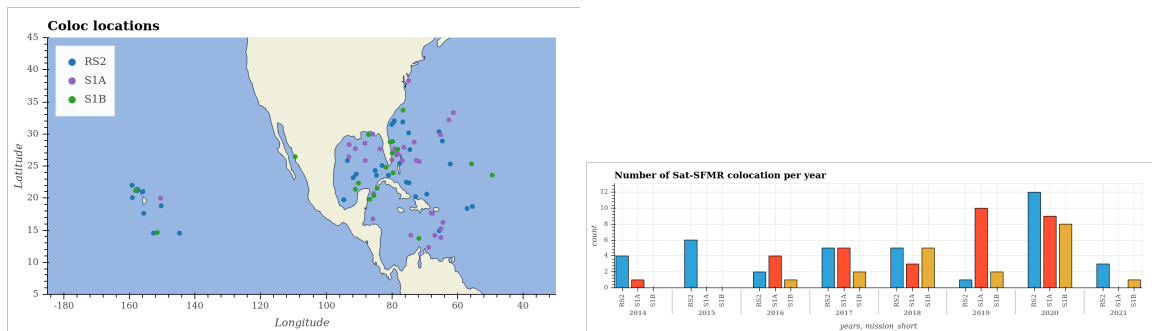

Figure 2.2: Status of collocated dataset between CyclObs SAR data and SFMR wind and rain products as provided by NOO/NESDIS group. A color code is used to discriminate the three SAR mission available in the database. (Left) Location of collocation. (Right) Time of collocation

2.2. Wind Speed comparisons

2.2.1. Summary
To be done

2.2.2. Impact of parameters
This section presents the comparison results and details the impact of various parameters on the wind speed performance of Level-2 CyclObs product as obtained during the validation exercise.

SFMR product type
To be done

Collocation time difference
We only consider SFMR/SAR couples within 2 hours. However and in spite of the collocation method to take into account for TC displacement with respect to time (because the vortex is rotating and the intensity can change very fast), the time difference can impact the comparison (see discussion in section 2.1.1).

When SFMR/SAR couples within 2 hours (i.e. $\Delta T < 2$ hours) , the number of collocations is 15749 and SFMR wind speed span between 5 and 80 m/s. The comparison yield to a bias of about 1 m/s, a standard deviation of about 5 m/s, a scatter index of 29% and a correlation of 0.8. When narrowing the time window to $\Delta T < 2$ hours and $\Delta T < 30$ min, the number of collocated points drops to 11648 (about 26% filtered) and 9527(about 39% filtered) respectively. This also improves the comparison with an observed decrease of all the parameters, excepted the correlation (negligible improvement). For $\Delta T < 30$ min bias of about 0.4 m/s, a standard deviation of about 5 m/s, a scatter index of 28% and a correlation of 0.8. To note these values are quite in line with the results published by . They considered much less data, applied the same algorithm and found a bias of 0.2 m/s, a standard deviation of about 5 m/s and a slightly better correlation of about 0.9.

Hereafter, unless explicitly indicated, we only use data collocated with a $\Delta T < 30$ min.
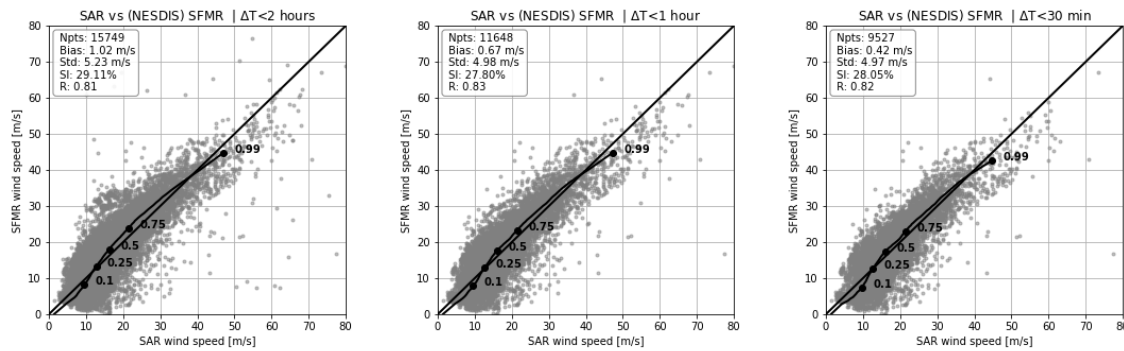
Figure 2.3: Comparison between all SAR derived wind speed from CYMS products and SFMR wind speed for rain rates lower than 5 mm/hr after collocation for different filtering thresholds with respect to time. Left: Time difference is less than 2 hours; Middle : Time difference is less than 1 hour; Right: Time difference is less than 30 minutes.
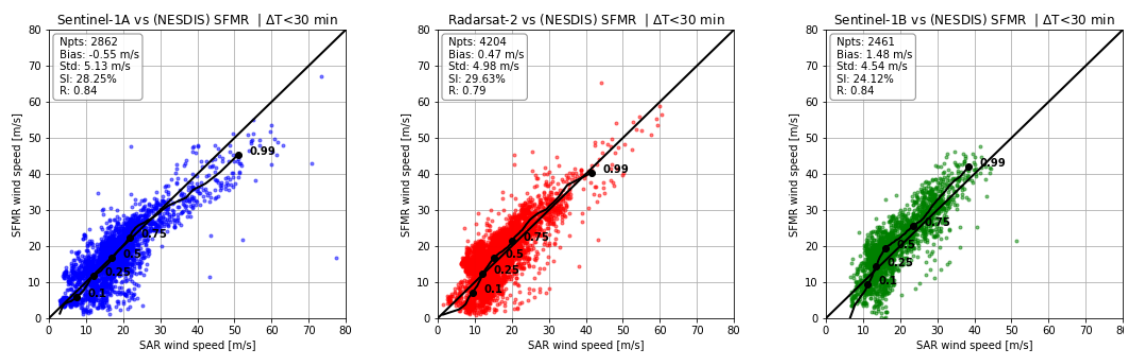

Figure 2.4: Comparison between SAR derived wind speed from CYMS products and SFMR wind speed for rain rates lower than 5 mm/hr after collocation for each of the SAR missions. Time difference is less than 30 minutes. Left: Sentinel-1; Middle : Radarsat-2; Right: Sentinel-1B.

SAR sensors

The analysis can be split with respect to the SAR sensor to possibly assess each sensor performance. Figure 2.4 presents the results for Sentinel-1A (left plot), Radarsat-2 (middle plot) and Sentinel-1B (right plot). Radarsat-2, the oldest sensor, provides most of the collocations (4204), whereas Sentinel-1A and Sentinel-1B roughly provide the same number (2862 for Sentinel-1A and 2461 for Sentinel-1B). As observed, the three comparisons yield to quite different results. For Sentinel-1A, a part from correlation coefficient, scatter index, standard deviation that are very similar to the overall (all SAR together) statistics, the comparison reveals an overall negative bias (about -0.5 m/s) and significant overestimation (i.e. positive bias) of the wind speeds for SFMR wind speeds larger than 30 m/s. Radarsat-2 performances are in agreement with the overall statistics and the direct comparison does not reveal a particular overestimation of the wind speed for stronger wind speeds. However, the scatter index is found to be larger than for Sentinel-1A and -1B. For Sentinel-1B, a part from correlation coefficient, scatter index, standard deviation that are very similar to the overall (all SAR together) statistics, the comparison reveals an overall positive bias (about 1.5 m/s). Very few measurements are available for wind speeds larger than 30 m/s, but an underestimation of SAR wind speeds is also observed.

Incidence angle

The analysis can also be performed as a function of incidence angle. This is a key parameter as the relationships used between the radar signal and the wind speed and direction depends on the incidence angle and SAR missions considered here have incidence angles ranging from 20 to 50 degrees.

Overall, when the 3 SAR measurements are merged, the bias is found to decrease with respect to incidence angle going from positive bias (about 2.5 m/s) at low incidence angles (20-30 degrees) and negative bias (about 2 m/s) at large incidence angles (40-50 degrees) and almost 0 m/s for medium
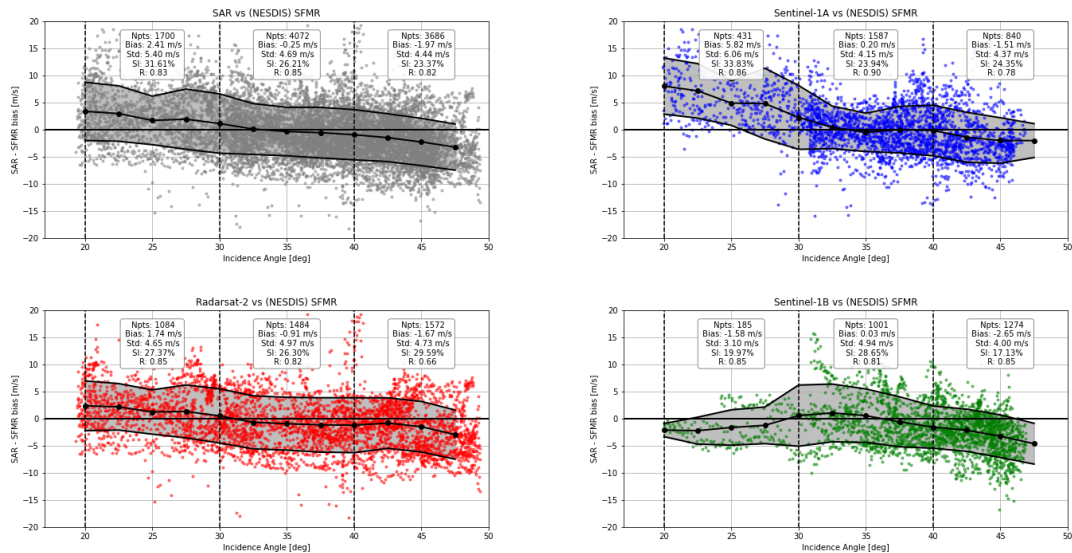
Figure 2.5: SAR derived wind speed from CYMS products minus SFMR wind speed for rain rates lower than 5 mm/hr after collocation for all and each of the SAR missions with respect to incidence angle. Top left: All SAR missions; Top right: Sentinel-1A; Bottom left: Radarsat-2; Bottom right: Sentinel-1B.

incidence angles (30-40 degrees). This trend is more pronounced for Sentinel-1A, than for Radarsat-2 and significantly stronger for low incidence angles (20-30 degrees) where the positive bias can reach about 6 m/s. The trend for Sentinel-1B is quite different for the low incidence angle with negative bias at low incidence angles (20-30 degrees).

The difference between obtained between the different sensors with respect to incidence angle suggest that they are not properly inter-calibrated. In the algorithm, a common set of GMFs (one for co- and one cross-polarization channels) to relate the radar signal to the wind with respect to incidence angle is used for the three SAR. As a result, if the sensors are not properly inter-calibrated, then the use of common GMFs will lead to different performances.

As the bias has been found to decrease with respect to incidence angle for all sensors, the dependency observed with respect to incidence angle certainly needs to be revised. The significant difference in the bias obtained with Sentinel-1A with respect to the two other SAR indicates a specific issue to be further investigate for this sensor. Also, because Radarsat-2 acquisition modes used in CyclObs cover incidence angles larger than 47 degrees (maximum angle for Sentinel-1 missions) a specific attention has to be paid for deriving a GMF up to 50 degrees.

Sentinel-1 acquisition modes and processing parameters

The processing parameters of Sentinel-1 A and B have been updated at different times since the launch of the two sensors. Among these parameters, the Elevation Antenna Pattern (EAP) and the Noise Equivalent Sigma Zero (NESZ) have a significant impact on the NRCS. This is particularly true for the cross-polarization channel whose magnitude is much less than for co-polarization channel. In addition, these changes do not occur at the same time for both sensors and the two acquisition modes considered here (EW and IW). The tracking of these changes can be found on https://qc.sentinel1.copernicus.eu/

To assess the impact of these changes, the previous comparisons are broken down with respect to acquisition time and mode. Here, the separation time is chosen to correspond to the most recent significant change. Figure 2.6 presents the wind speed difference between SAR and SFMR for Sentinel-1 A (top panels) and Sentinel-1 B (bottom panels) before and after the separation time in the processing parameters. As observed, the performances are different with respect to sensors, mode and time. However, given the small amount of data, this is difficult to conclude accurately. Using other data for comparison, will help to refine this analysis (see next sections).
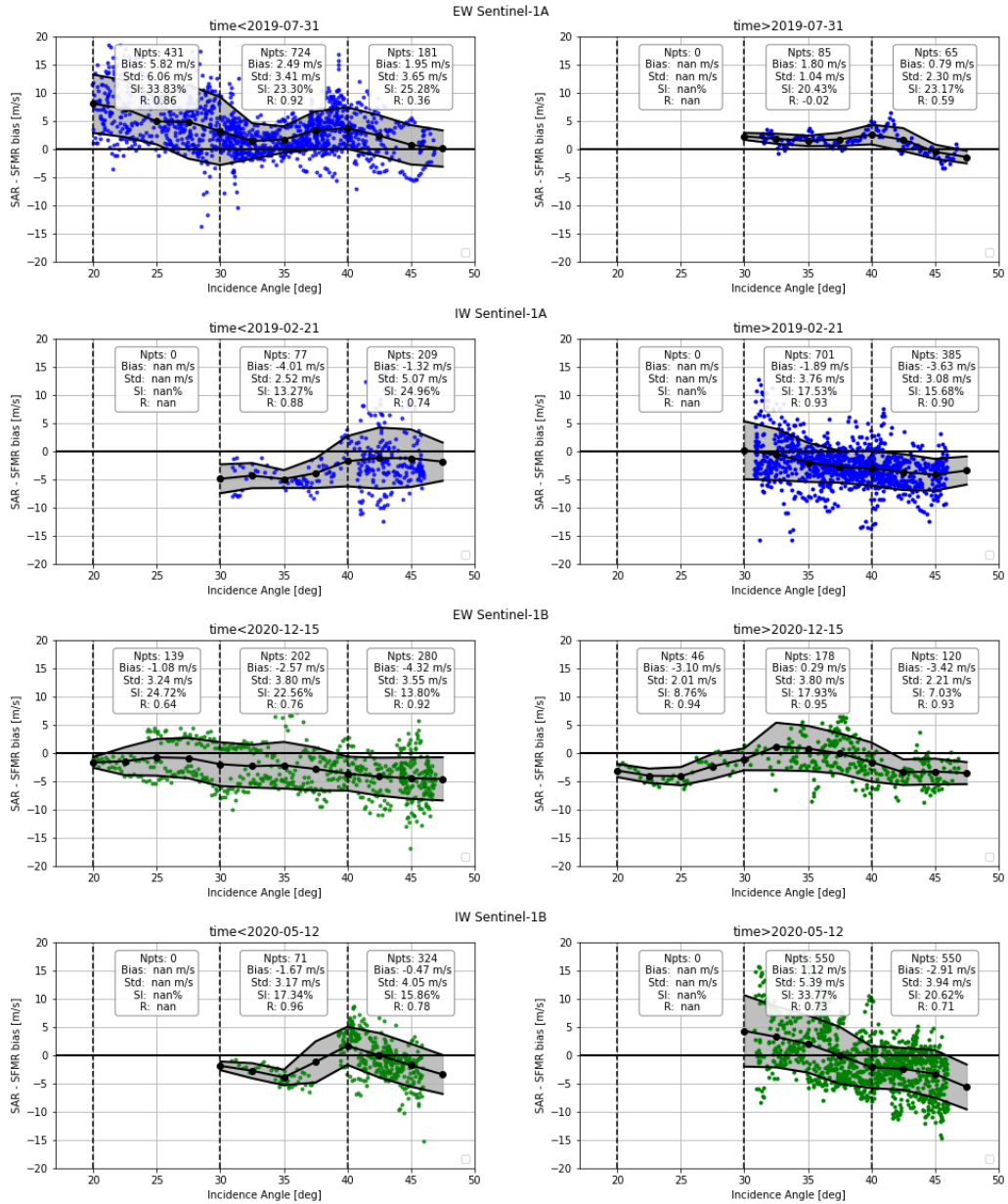
Figure 2.6: SAR derived wind speed from CYMS products minus SFMR wind speed for rain rates lower than 5 mm/hr after collocation for Sentinel-1A and Sentinel-1B missions with respect to incidence angle, acquisition modes and processing date. First line: Sentinel-1A EW; Second line: Sentinel-1A IW; Third line: Sentinel-1B EW; fourth line: Sentinel-1B IW. Left column : data acquired before the last key processing parameters update. Right column : data acquired after the last key processing parameters update.

3

SAR versus SMAP : Overview

3.1. Collocation

This section presents the collocation method and collocated data set available for comparisons.

3.1.1. Method

The collocation approach is chosen is more straightforward than for SFMR. All SMAP/SAR match-ups with a collocation time lower than 30 minutes are considered as collocated in both time and space.

In particular, there was no attempt to correct for the TC evolution such as the TC displacement(translation, rotation) or for the TC evolution (intensity and shape change).

3.1.2. Dataset

3.2. Wind Speed comparisons

3.2.1. Summary

SMAP and SAR collocations exercise led to more than 45000 match-ups. The comparison between the wind speed from the two types of sensors when SAR data are merged can be summarized as:

- a bias of 0.2 m/s, a standard deviation of 2.6 m/s and a scattering index of 20% are obtained.
- a bias with respect to incidence angle is found leading to wind speed overestimates at low incidence angles (0.7 m/s for incidence angles <30 degrees) and underestimates at high incidence angles (-0.9 m/s for incidence angles>40 degrees).

When analysing Level-2 performances for each sensor we observe that

- Sentinel-1A

    - overestimates the strongest wind speeds.
    - overall wind speed overestimate is mainly due to the bias obtained for low incidence angle (1.5 m/s for incidence angles lower than 30 degrees) when Sentinel-1A is operating in EW acquisition mode.

- Radarsat-2

    - underestimates the strongest wind speeds.
    - Radarsat-2 performances are particularly impacted by the high incidence angle measurements.

- Sentinel-1B

    - performances seems very close to Sentinel-1A.
    - We observe the same bias trend with respect to incidence angle but less pronounced (0.7 m/s for incidence angles lower than 30 degrees)
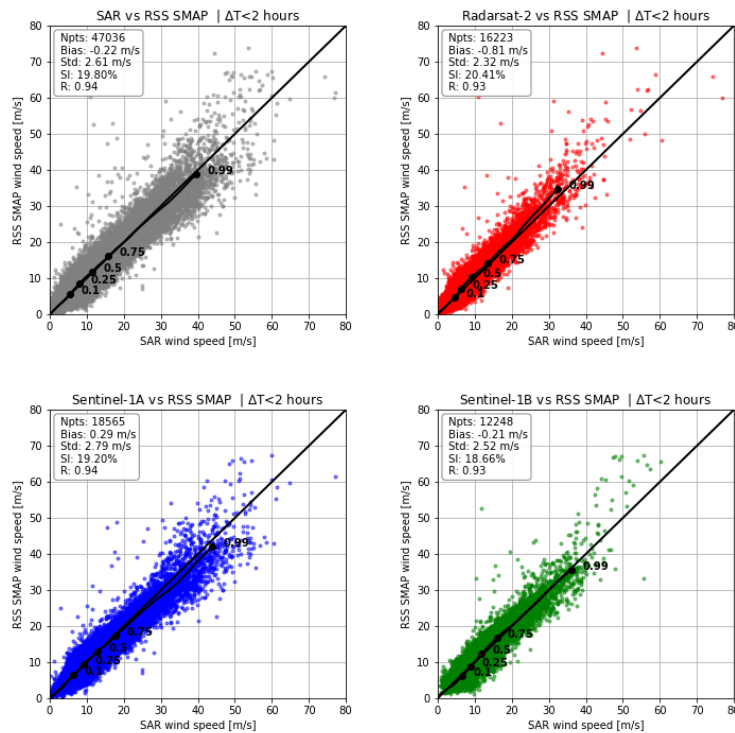
Figure 3.1: Comparison between SAR derived wind speed from CYMS products and SMAP wind speed after collocation for each of the SAR missions. Time difference is less than 30 minutes. Top left: All; Top right: Sentinel-1; Bottom Left : Radarsat-2; Bottom Right: Sentinel-1B.

A detailed analysis of Sentinel-1 mission also reveals that the acquisition time and the acquisition mode impact the Level-2 product performances. In particular, the incidence angle effect has been reduced with the last updates of the elevation antenna gain pattern and noise annotated in the product. This is mostly significant for low incidence angles when Sentinel-1A is operated in EW mode.

3.2.2. Direct comparisons
When all SAR are merged, the obtained results are -0.22 m/s and 2.61 m/s, respectively for the bias and standard deviation.

3.2.3. Impact of parameters
This section presents the comparison results and details the impact of various parameters on the wind speed performance of Level-2 CyclObs product as obtained during the validation exercise.

SAR sensors
When splitting the results with respect to each of the SAR sensors available, significant differences can be observed. Radarsat-2 have the largest value of bias (-0.81 m/s) which is negative, indicating that the algorithm underestimates the strongest wind speeds estimated with Radarsat-2. Sentinel-1 performances yield to the largest standard deviation and indicate that the algorithm overestimates the strongest wind speeds. Overall, this analysis reveal that Sentinel-1B has the best results when compared to SMAP. However, Sentinel-1B has also the smaller data set and much less observations for the strongest wind speeds than the two other sensors. The performances obtained for Sentinel-1A and Radardat-2 against SMAP are in line with the comparisons against SFMR. In the contrary, Sentinel-1B performances against SMFR were the poorest with a bias of 1.48 m/s; but also obtained with a significant data set.
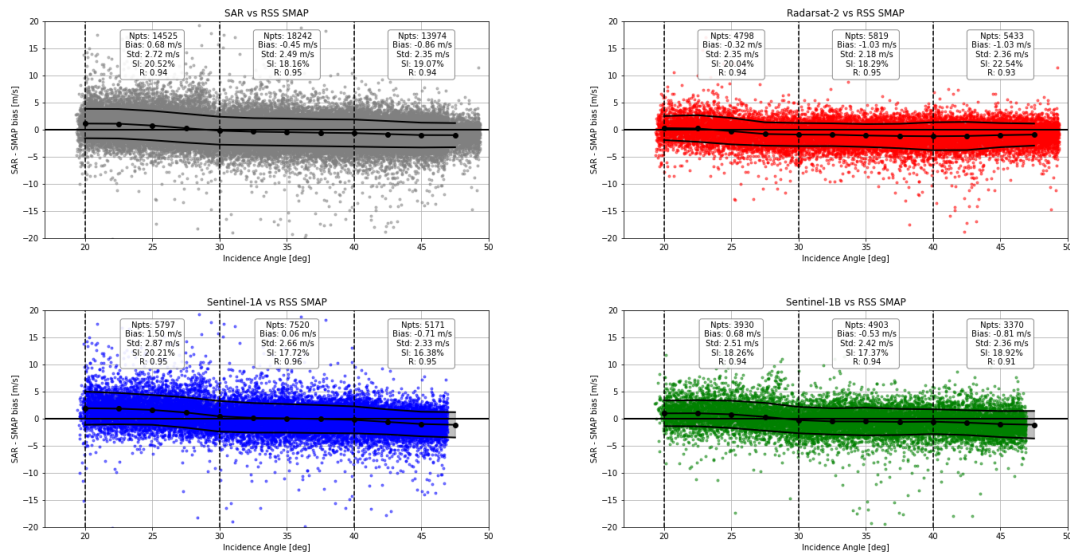
Figure 3.2: SAR derived wind speed from CYMS products minus SMAP wind speed after collocation for all and each of the SAR missions with respect to incidence angle. Top left: All SAR missions; Top right: Sentinel-1A; Bottom left: Radarsat-2; Bottom right: Sentinel-1B.

Incidence angle

Overall, when the 3 SAR measurements are merged, the bias is found to decrease with respect to incidence angle going from positive bias (about 0.7 m/s) at low incidence angles (20-30 degrees) and negative bias (about -0.9 m/s) at large incidence angles (40-50 degrees) and 0.5 m/s for medium incidence angles (30-40 degrees). This trend is line with comparisons against SFMR presented in section 2.2.2.4 but less pronounced.

This trend is more pronounced for Sentinel-1A, than for Radarsat-2 and Sentinel-1B significantly stronger for low incidence angles (20-30 degrees) where the mean positive bias can reach about 1.5 m/s. Both Sentinel-1 missions overestimate the wind speed as compared to SMAP for low incidence angles with a small negative bias for high incidence angles. Radarsat-2 seems to underestimate the wind speeds; in particular for incidence angles larger than 25 degrees.

Sentinel-1 acquisition modes and processing parameters

As for SFMR, this sections proposes to go further in these analysis and to investigate the possible impact of the acquisition mode and time (with respect to changes in the processing parameters). To assess the impact of these changes, the previous comparisons are broken down with respect to acquisition time and mode. Here, the separation time is chosen to correspond to the most recent significant change.

Figure 3.3 presents the wind speed difference between SAR and SMAP for Sentinel-1 A (top panels) and Sentinel-1 B (bottom panels) before and after the separation time in the processing parameters. This analysis confirms that the Level-1 product processing changes impact the Level-2 performances and that the data quality is not the same with respect to sensor and acquisition mode. For S-1A and S1-B operating in EW mode, the performances are improved. This is particularly true for the low incidence angles. For S-1A and S1-B operating in IW the number of collocation is less but a significant decrease in the performances is observed. for S-1A, large incidence angles seem more impacted. For S-1B, the whole incidence angle range is impacted with a mean bias larger than 2 m/s.
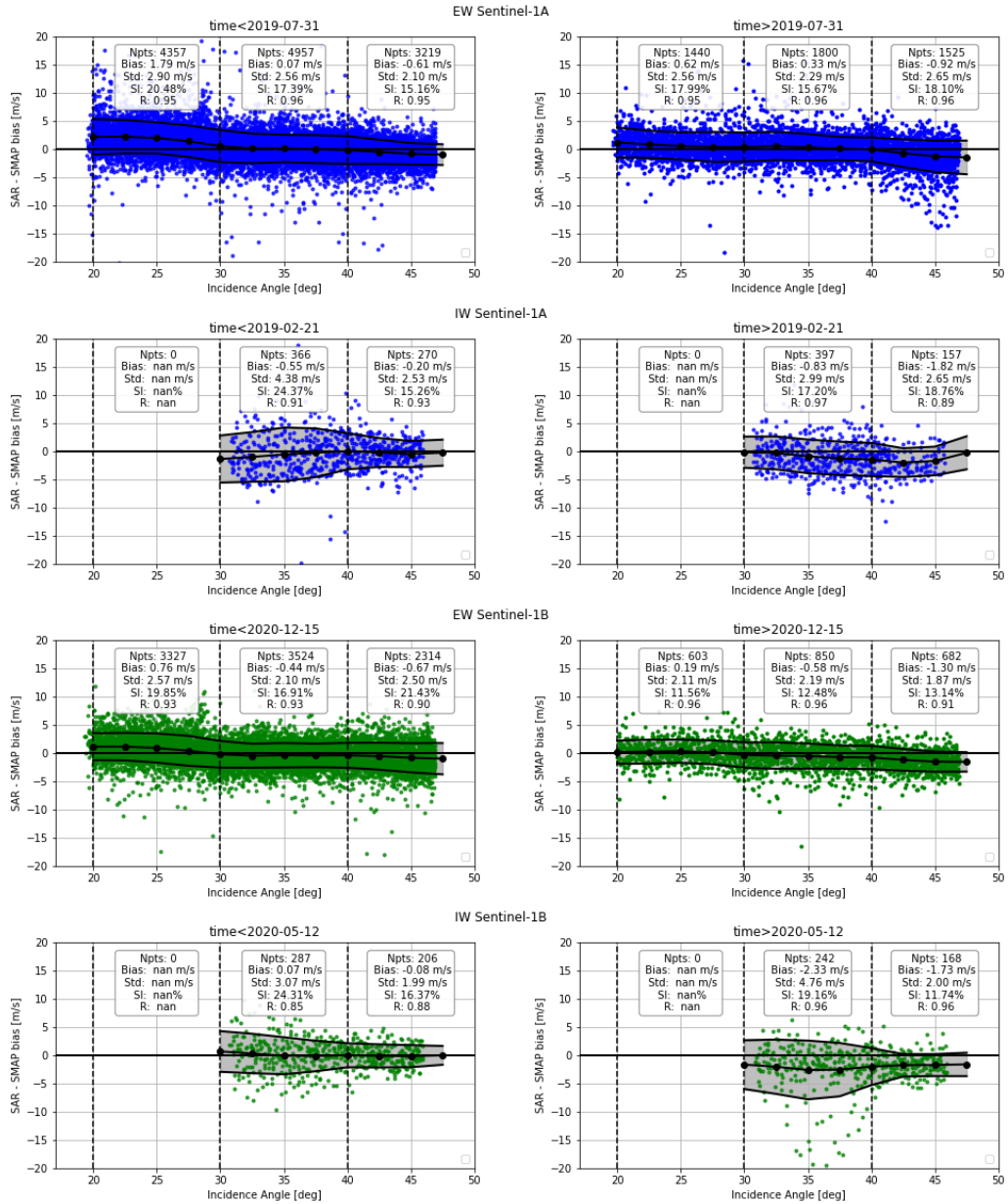
Figure 3.3: SAR derived wind speed from CYMS products minus SMAP wind speed for rain rates lower than 5 mm/hr after collocation for Sentinel-1A and Sentinel-1B missions with respect to incidence angle, acquisition modes and processing date. First line: Sentinel-1A EW; Second line: Sentinel-1A IW; Third line: Sentinel-1B EW; fourth line: Sentinel-1B IW. Left column : data acquired before the last key processing parameters update. Right column : data acquired after the last key processing parameters update.

4
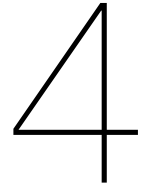
SAR versus SAR : Overview

Radarsat-2 and Sentinel-1 orbit parameters allow for having cross-over between the two missions. This chapter relies on this cross-over to assess the consistency between the SAR wind estimates obtained between Radarsat-2 and Sentinel-1A, and Radarsat-2 and Sentinel-1B.

4.1. Collocation

This section presents the collocation method and collocated data set available for comparisons.

4.1.1. Method

In the contrary of SFMR and applying the same method than for SMAP, the collocation approach is straightforward. All S1A/RS2 and S1B/RS2 match-ups with a collocation time lower than 30 minutes are considered as collocated in both time and space.

In particular, there was no attempt to correct for the TC evolution such as the TC displacement (translation, rotation) or for the TC evolution (intensity and shape change).

4.1.2. Dataset

Following the method described in section 4.1.1, we obtain 22 collocations int the 4 main area North Atlantic ocean (NA: 18%), North East Pacific ocean (NE: 18%), North West Pacific ocean (NWP: 36%) and South Indian ocean (SI: 27%):

- 15 S1A/RS2 collocations
- 7 S1B/RS2 collocations

All TC categories, excepted the category-5 are sampled :

- for S1A/RS2,

    - $<$cat-1: 4
    - cat-1: 2,
    - cat-2: 1,
    - cat-3: 2,
    - cat-4: 6,
    - cat-5: 0;

- for S1B/RS2,

    - $<$cat-1: 2,
    - cat-1: 1,
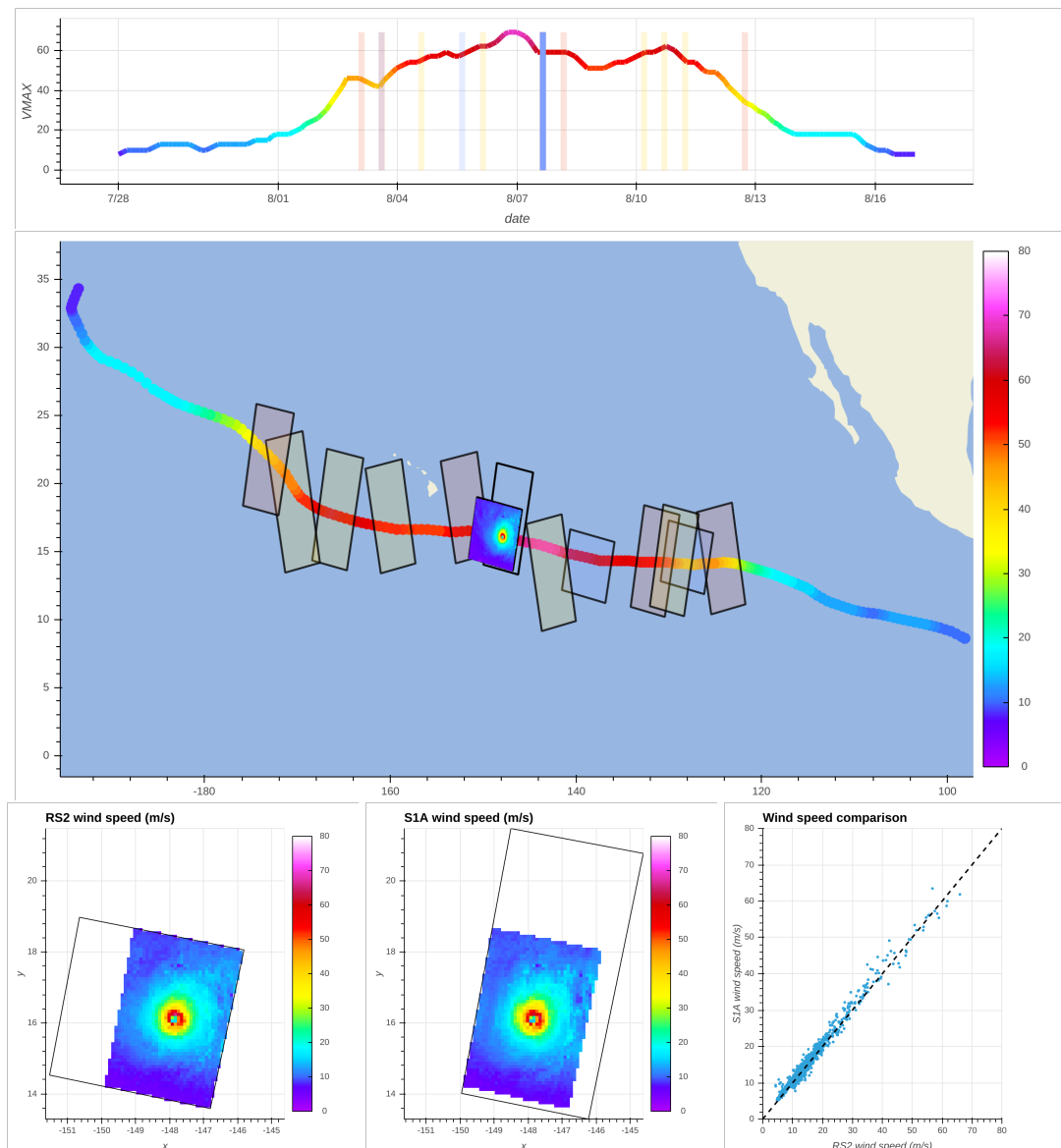   - cat-2: 2,
    - cat-3: 2,
    - cat-4: 0,
    - cat-5: 0,

Figure 4.1: Hector TC (2018). Top: Evolution of 1-min maximum sustained wind speed with respect to time as given by ATCF TC track. Vertical bars indicates time of SAR acquisition of this TC. Middle: Map of the TC track and SAR acquisition footprints. Bottom-Left: Map of wind speed values from Radarsat-2 collocated with Sentinel-1A ; Bottom-middle: Map of wind speed values from Sentinel-1A collocated with Radarsat-2; Bottom-right: Direct comparison between Radarsat-2 and Sentinel-1A collocated wind speed estimates.

4.2. Wind speed comparisons

4.2.1. summary
To be done

4.2.2. Case study
4.2.3 Although a general agreement is found (see next section), a case-by-case analysis also revealed very different agreement between Radarsat-2 and Sentinel-1 mission. This section illustrates different case-study.

Hector TC: Sentinel-1A and Radarsat-2
Hector was a cat-4 TC occurred in 2018 in the north-east and central Pacific. For this TC, 13 SAR observations have been obtained and Hector reached its maximum intensity around 00 UTC the 7th of August 2018 (see Figure 4.1). The collocated SAR data were acquired the 7th of August 2018 around 15:45 UTC with a time difference of 2 minutes and 10 seconds. At that time the maximum wind speed was about 60 m/s (from TC track), Hector being a category-3 hurricane. The location of these 2 acquisitions can be seen on Figure 4.1, where the wind map corresponds to Radarsat-2 derived wind speed.

As shown on Figure 4.1, they both observed the TC eye and surrounding area associated with strongest wind speed values. On Figure 4.1, only the common area between the two acquisitions is presented. The area of strong wind is located in the near-range and in the middle-range of Radarsat-2 and Sentinel-1A subswath, respectively. This corresponds to incidence angles of about 30 degrees for RS2 and 35 degrees for S1A. For each map, the black rectangle stands for the full acquisition limit.

The direct comparison between the two sensor wind speed estimates is shown on the right panel of Figure 4.1 and yields to bias less than 0.4 m/s with standard deviation of 1.0 m/s. This case reflects a case of remarkable agreement between the two missions. To note, in this example, the strongest wind have been acquired at incidence angles corresponding to the best performances for Sentinel-1A and Radarsat-2 when compared to SFMR and SMAP and where changes in the Sentinel-1 Level-1 processor has the minimum impact for S1A. For these two Level-2 wind product, the Tropical Cyclone Analysis product that gathers TC parameters gives 123 knts and 119 knts for Radarsat-2 and Sentinel-1A, respectively while ATCF TC best-track gives 115 knts.

Maysak TC: Sentinel-1B and Radarsat-2
Maysak was a cat-3 TC occurred in 2020 in the north-west Pacific. For this TC, only 3 SAR observations have been obtained and Maysak reached its maximum intensity around 00 UTC the 1st of September 2020 (see Figure 4.2). The collocated SAR data were acquired the 1st of September 2020 around 21:30 UTC with a time difference of 7 minutes and 23 seconds. At that time the maximum wind speed was about 55 m/s (from TC track), Maysak being a category-3 typhoon. The location of these 2 acquisitions can be seen on Figure 4.2, where the wind map corresponds to Radarsat-2 derived wind speed.

As shown on Figure 4.2, they both observed the TC eye and surrounding area associated with strongest wind speed values. On Figure 4.2, only the common area between the two acquisitions is presented. The area of strong wind is located in the near-range or in the far-range of Radarsat-2 and Sentinel-1B subswath, respectively. This corresponds to incidence angles of about 35 degrees for RS2 and 40 degrees for S1B. For each map, the black rectangle stands for the full acquisition limit.

The direct comparison between the two sensor wind speed estimates is shown on the right panel of Figure 4.2 and yields to bias of about 2.2 m/s with standard deviation of about 3.0 m/s. This case is an illustration of the possible inconsistency observed between two Level-2 wind products originated from two different sensors sampling the same TC at the same time. To note, in this example the strongest wind have been acquired at incidence angles corresponding to the best performances for Radarsat-2 but to underestimated wind speed values for Sentinel-1B when compared to SFMR (see Figure 2.5) and SMAP (see Figure 3.2). For these two Level-2 wind product, the Tropical Cyclone Analysis product that gathers TC parameters gives 80 kts and 67 kts for Radarsat-2 and Sentinel-1B, respectively while ATCF TC best-track gives 115 kts at 18:00 UTC for the 1st and 105 kts at 00:00 UTC for the 2nd of September 2020. This confirms the underestimated wind speed from Sentinel-1B in this case. Altough in better agreement, the maximum sustained wind speed estimated from Radarsat-2 acquisition also seems to be slightly underestimated.
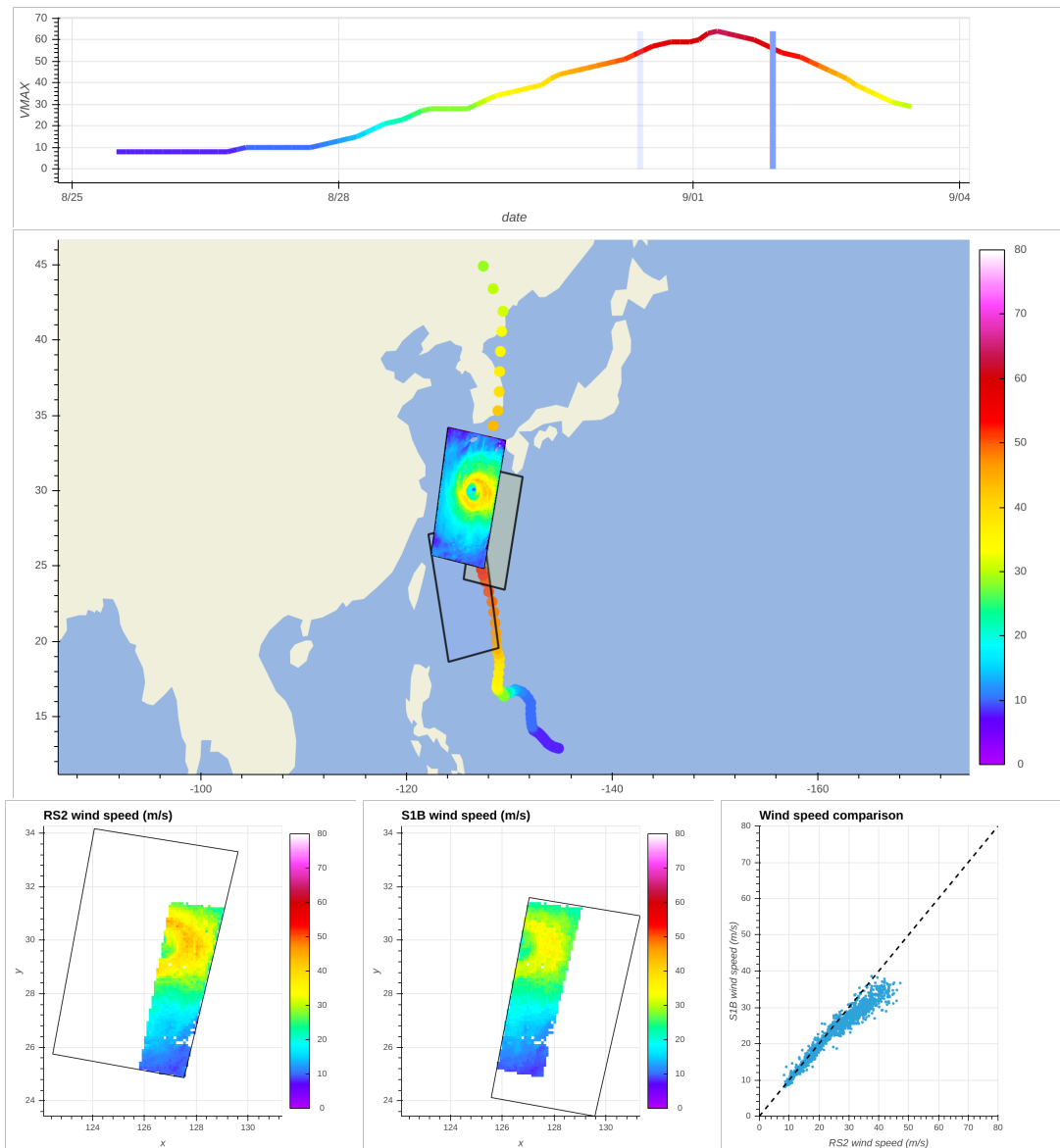
Figure 4.2: Maysak TC (2020). Top: Evolution of 1-min maximum sustained wind speed with respect to time as given by ATCF TC track. Vertical bars indicates time of SAR acquisition of this TC. Middle: Map of the TC track and SAR acquisition footprints. Bottom-Left: Map of wind speed values from Radarsat-2 collocated with Sentinel-1B ; Bottom-middle: Map of wind speed values from Sentinel-1B collocated with Radarsat-2; Bottom-right: Direct comparison between Radarsat-2 and Sentinel-1B collocated wind speed estimates.

Batsirai TC: Sentinel-1A and Radarsat-2

Batsirai was a cat-4 TC occurred in 2022 in the South Indian ocean basin. For this TC, 9 SAR observations have been obtained and Batsirai reached its maximum intensity around 06 UTC the 2nd of February 2022 (see Figure 4.3). The collocated SAR data were acquired the 30 of January 2022 around 01:00 UTC with a time difference of 19 minutes and 34 seconds. At that time the maximum wind speed was about 50 m/s (from TC track), Batsirai being a category-2/3 cyclone. The location of these 2 acquisitions can be seen on Figure 4.3, where the wind map corresponds to Radarsat-2 derived wind speed.

As shown on Figure 4.3, they both observed the TC eye and surrounding area associated with strongest wind speed values. On Figure 4.3, only the common area between the two acquisitions is presented. The area of strong wind is located in the far-range or in the near-range of Radarsat-2 and Sentinel-1A subswath, respectively. This corresponds to incidence angles of about 40 degrees for RS2 and 25 degrees for S1B. For each map, the black rectangle stands for the full acquisition limit.

The direct comparison between the two sensor wind speed estimates is shown on the right panel of Figure 4.3 and yields to bias of about -3.2 m/s with standard deviation of about 2.8 m/s. This case is an illustration of the possible inconsistency observed between two Level-2 wind products originated from two different sensors sampling the same TC at the same time. To note, in this example the strongest wind have been acquired at incidence angles corresponding to the poorest performances for both Radarsat-2 (largest incidence angles) and Sentinel-1A (lowest incidence angles) when compared to SFMR (see Figure 2.5) and SMAP (see Figure 3.2). For these two Level-2 wind product, the Tropical Cyclone Analysis product that gathers TC parameters gives 74 kts and 124 kts for Radarsat-2 and Sentinel-1A, respectively while ATCF TC best-track gives 95 kts at 00:00 UTC and 100 kts at 06:00 UTC for the 30 of January 2022. This confirms the strong underestimated wind speeds from Radarsat-2 and the strong overestimated wind speeds from Sentinel-1A in this case.
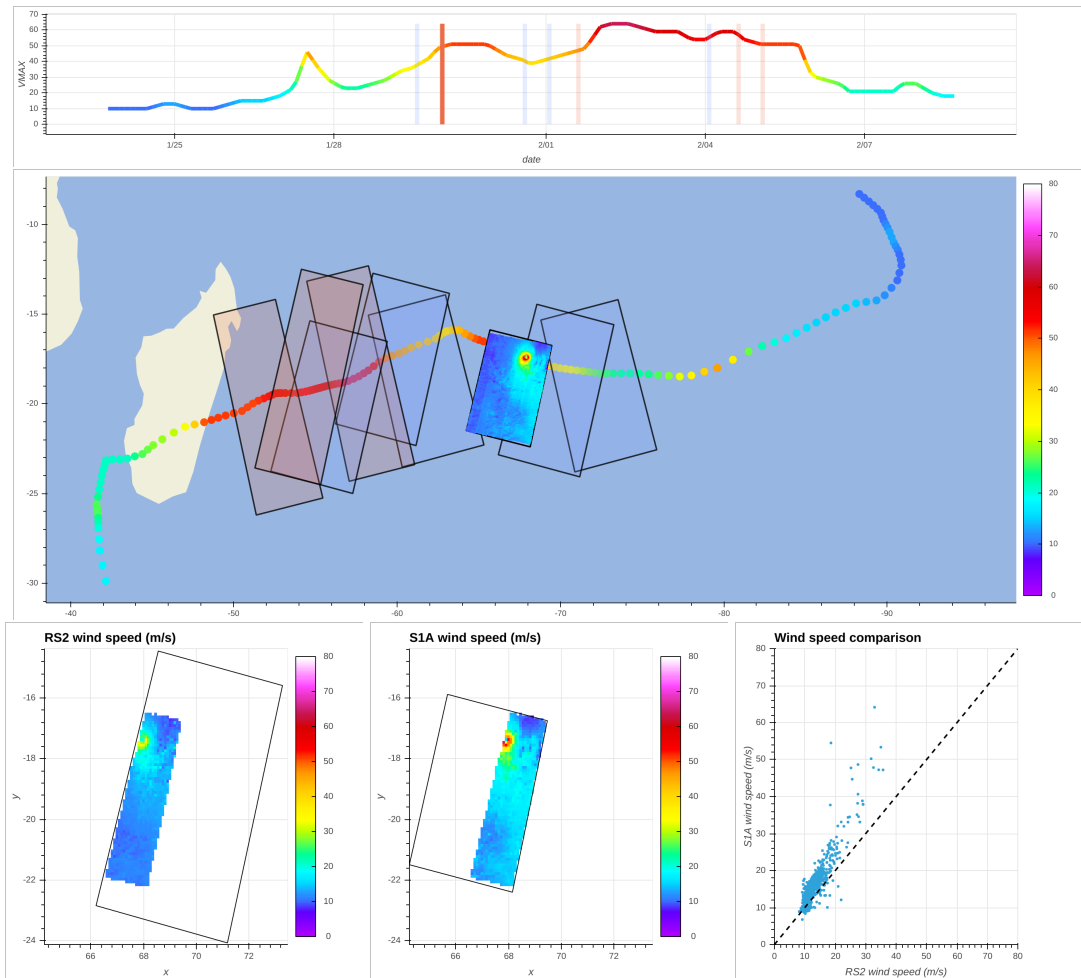

Figure 4.3: Batsirai TC (2022). Top: Evolution of 1-min maximum sustained wind speed with respect to time as given by ATCF TC track. Vertical bars indicates time of SAR acquisition of this TC. Middle: Map of the TC track and SAR acquisition footprints. Bottom-Left: Map of wind speed values from Radarsat-2 collocated with Sentinel-1A ; Bottom-middle: Map of wind speed values from Sentinel-1A collocated with Radarsat-2; Bottom-right: Direct comparison between Radarsat-2 and Sentinel-1A collocated wind speed estimates.

This case is also an illustration of the collocation methodology limitation. Indeed during the separation time of about 20 min between the two acquisition times, the vortex has moved from about 9.7 km with a translation speed of about 8 m/s. This is illustrated on Figure 4.4, where the eye location can be observed on RS2 and S-1A cross-polarized NRCS maps. At that time Batsirai had a radius of maximum wind speed of about 11 km i.e. about the same than the translation distance, preventing for a direct comparison in the area of strongest wind speeds.
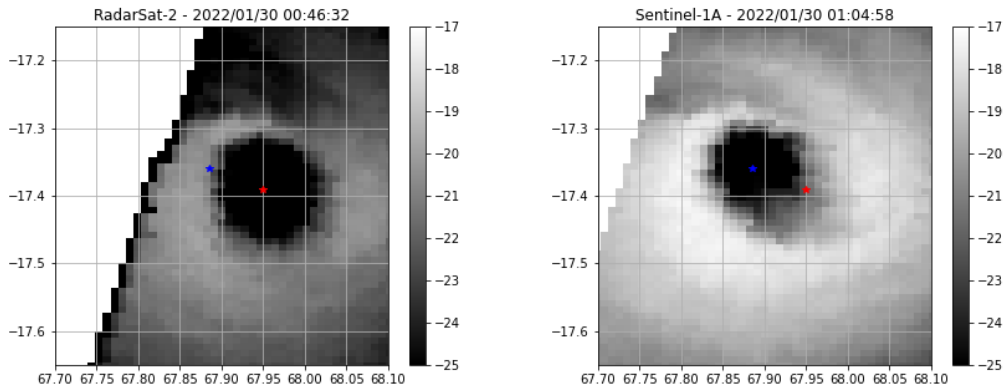
Figure 4.4: NRCS map in cross-polarization. Zoom on Batsirai TC eye observed on 2022/01/30 with Radarsat-2 at 00:46:32 UTC (Left) and Sentinel-1A at 01:04:58 UTC (Right).

4.2.3. Statistical Analysis

The statistical analysis confirms significant differences between Radarsat-2 and Sentinel-1 missions. This is particularly true for the strongest values of wind speed. As obtained, Radarsat-2 wind speed estimates seems to be larger than Sentinel-1B wind speeds and lower than Sentinel-1A wind speeds. However, as illustrated in the previous chapters when comparing SAR wind speeds to SMAP and SFMR and in the previous section , SAR performances depends on incidence angles. As a results when comparing two SAR images the two incidence angle range needs to be taken into account.

We thus compute the mean differences obtained for each images with respect to incidence angles ranging from 17 degrees to 50 degrees with a step of 1 degrees for both S1A/RS2 and S1B/RS2 col-located dataset. The results are presented Figure 4.5. For S1A/RS2, this analysis confirms an overall overestimate of the wind speeds for Sentinel-1A. This is particularly true when Radarsat-2 incidence angles are large and Sentinel-1A incidence angle are low. Here we only have one collocation with S1A acquisition in IW mode. It is thus difficult to get solid conclusion for this mode. However, in this case, Sentinel-A seems to underestimate winds compared to Radarsat-2. For S1B/RS2, this analysis confirms an overall underestimate of the wind speeds for Sentinel-1B. However, most of the data are acquired when Sentinel-1B and Radarsat-2 images are acquired with high incidence angle and low incidence angle, respectively. This prevents to conclude for the other incidence angle combinations.
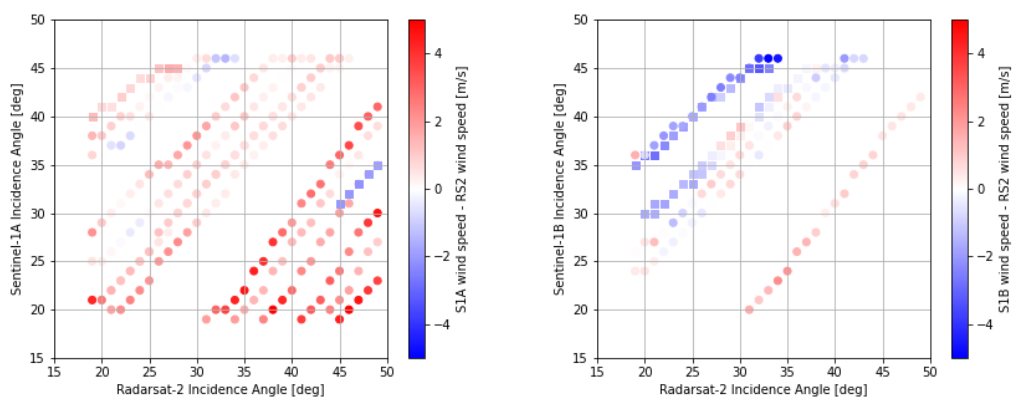

Figure 4.5: Mean wind speed difference between Sentinel-1 and Rardarsat-2 missions with respect to incidence angles of the two SAR missions. dots and squares stand for Sentinel-1 data acquired in EW and IW modes, respectively. Left: Sentinel-1A and Radarsat-2. Right: Sentinel-1B and Radarsat-2.

Bibliography

Klotz, B. W. and Uhlhorn, E. W. (2014). Improved Stepped Frequency Microwave Radiometer Tropical Cyclone Surface Winds in Heavy Precipitation. *Journal of Atmospheric and Oceanic Technology*, 31(11):2392–2408.

Meissner, T., Ricciardulli, L., and Wentz, F. J. (2017). Capability of the SMAP Mission to Measure Ocean Surface Winds in Storms. *Bulletin of the American Meteorological Society*, 98(8):1660–1677.

Meissner, T. and Wentz, F. J. (2012). The Emissivity of the Ocean Surface Between 6 and 90 GHz Over a Large Range of Wind Speeds and Earth Incidence Angles. *IEEE Transactions on Geoscience and Remote Sensing*, 50(8):3004–3026.

Mouche, A., Chapron, B., Knaff, J., Zhao, Y., Zhang, B., and Combot, C. (2019). Copolarized and Cross‐Polarized SAR Measurements for High‐Resolution Description of Major Hurricane Wind Structures: Application to Irma Category 5 Hurricane. *Journal of Geophysical Research: Oceans*, 124(6):3905–3922.

Reul, N., Chapron, B., Zabolotskikh, E., Donlon, C., Mouche, A., Tenerelli, J., Collard, F., Piolle, J. F., Fore, A., Yueh, S., Cotton, J., Francis, P., Quilfen, Y., and Kudryavtsev, V. (2017). A New Generation of Tropical Cyclone Size Measurements from Space. *Bulletin of the American Meteorological Society*, 98(11):2367–2385.

Reul, N., Chapron, B., Zabolotskikh, E., Donlon, C., Quilfen, Y., Guimbard, S., and Piolle, J. (2016). A revised L-band radio-brightness sensitivity to extreme winds under Tropical Cyclones: the five year SMOS-storm database. *Remote Sensing of Environment*, 180:274–291.

Sapp, J., Alsweiss, S., Jelenak, Z., Chang, P., and Carswell, J. (2019). Stepped Frequency Microwave Radiometer Wind-Speed Retrieval Improvements. *Remote Sensing*, 11(3):214.

Stoffelen, A., Aaboe, S., Calvet, J.-C., Cotton, J., De Chiara, G., Saldaña, J. F., Mouche, A. A., Portabella, M., Scipal, K., and Wagner, W. (2017). Scientific developments and the eps-sg scatterometer. *IEEE Journal of Selected Topics in Applied Earth Observations and Remote Sensing*, 10(5):2086–2097.

Uhlhorn, E. W. and Black, P. G. (2003). Verification of Remotely Sensed Sea Surface Winds in Hurricanes. *Journal of Atmospheric and Oceanic Technology*, 20(1):99–116.

Uhlhorn, E. W., Black, P. G., Franklin, J. L., Goodberlet, M., Carswell, J., and Goldstein, A. S. (2007). Hurricane Surface Wind Measurements from an Operational Stepped Frequency Microwave Radiometer. *Monthly Weather Review*, 135(9):3070–3085.

Yueh, S. H., Fore, A. G., Tang, W., Hayashi, A., Stiles, B., Reul, N., Weng, Y., and Zhang, F. (2016). Smap l-band passive microwave observations of ocean surface wind during severe storms. *IEEE Transactions on Geoscience and Remote Sensing*, 54(12):7339–7350.

Zhang, B. and Perrie, W. (2012). Cross-Polarized Synthetic Aperture Radar: A New Potential Measurement Technique for Hurricanes. *Bulletin of the American Meteorological Society*, 93(4):531–541.